Electronic Supplementary Material (ESI) for Materials Horizons.
This journal is © The Royal Society of Chemistry 2019

Immersion Precipitation 3D Printing (*ip*3DP): Supporting Information

Rahul Karyappa[1], Akihiro Ohno[1], and Michinao Hashimoto[1,2,a)]

[1] Digital Manufacturing and Design (DManD) Centre, Singapore University of Technology and Design, 8, Somapah Road, Singapore 487372

[2] Pillar of Engineering Product Development, Singapore University of Technology and Design, 8, Somapah Road, Singapore 487372

[a)]Electronic mail: hashimoto@sutd.edu.sg

Supporting Fig. S1. A photograph of the direct ink writing (DIW) 3D printer and the pneumatic dispenser used in this study.

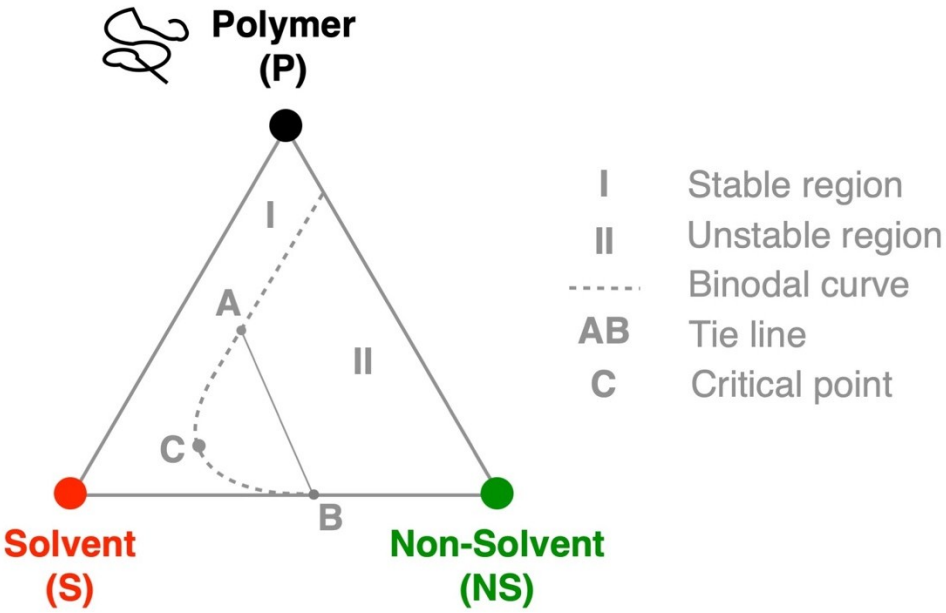

Supporting Fig. S2. Polymer-solvent-nonsolvent (P-S-NS) ternary phase diagram.

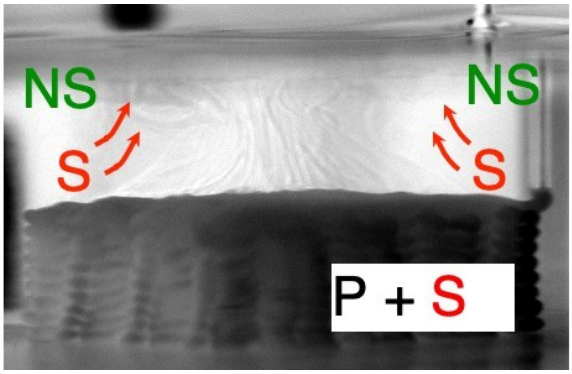

Supporting Fig. S3. An image showing immersion precipitation. The plumes of solvent (S) leaving polymer (P) and diffusing into the surrounding nonsolvent (NS) are visualized.

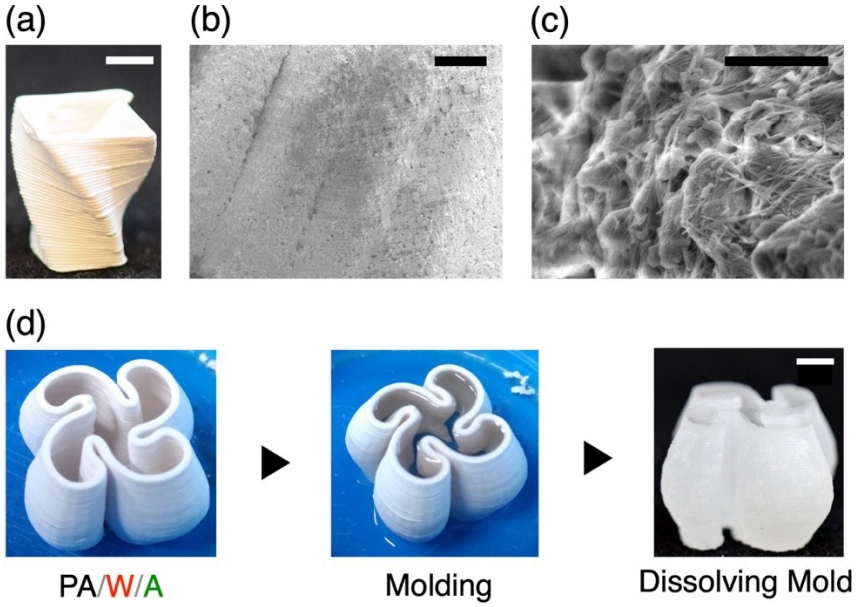

Supporting Fig. S4. (a) 3D structure of polyacrylate (PA) composite fabricated by *ip*3DP. (b) SEM image of surface of 3D structure. (c) SEM image of microstructures of the fracture surface. (d) Use of PA composite as a sacrificial material. The PA mold was printed by *ip*3DP, filled with PDMS, and dissolved in water. Scale bars = (a) 5 mm, (b) 200 μm, (c) 2 μm and (d) 5 mm.

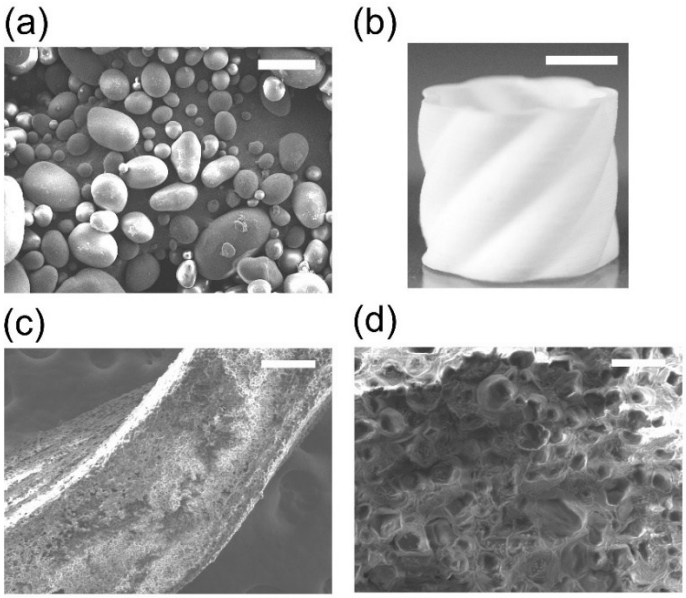

Supporting Fig. S5. (a) SEM image of starch used in the reinforcement of cellulose acetate (CA). (b) 3D model of starch-reinforced CA fabricated by *ip*3DP. (c-d) SEM images of microstructures of the fractured surface of starch-reinforced CA. Scale bars = (a) 50 μm, (b) 5 mm, (c) 200 μm and (d) 20 μm.

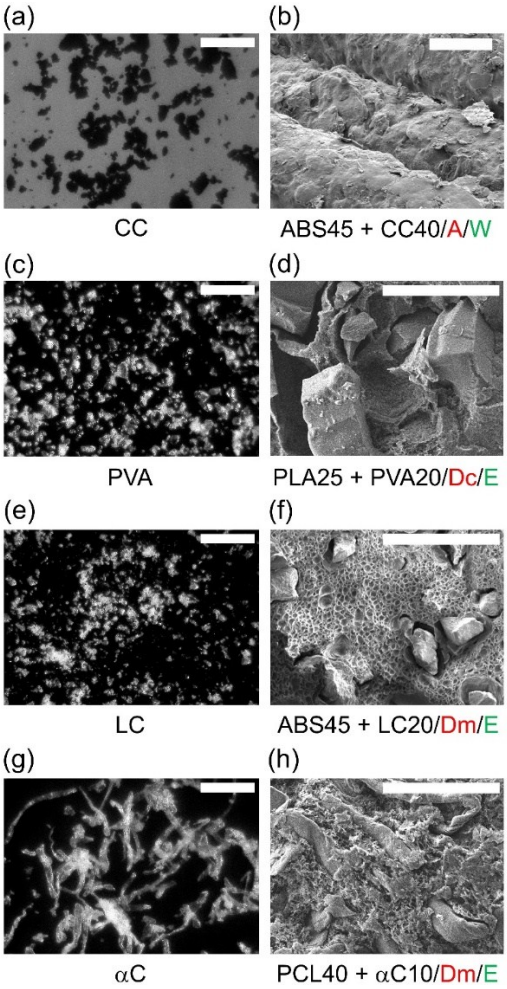

Supporting Fig. S6. (a, b) Optical micrograph of conductive carbon (CC), and SEM image of the interface of the 3D structure of CC-reinforced ABS45 printed in water. (c, d) Optical micrograph of polyvinyl alcohol (PVA), and SEM image of the internal microstructure of the fracture surface of the PVA-reinforced PLA25 printed in ethanol. (e, f) Optical micrograph of laponite clay (LC), and SEM image of the internal microstructure of the fracture surface of the LC-reinforced ABS45 printed in ethanol. (g, h) Optical micrograph of α-cellulose (αC) and SEM image of the internal microstructure of the fracture surface of the αC-reinforced PCL40 printed in ethanol. Scale bars = (a) 300 μm, (b) 100 μm, (c) 300 μm, (d) 100 μm, (e) 300 μm, (f) 100 μm, (g) 300 μm, and (h) 100 μm.

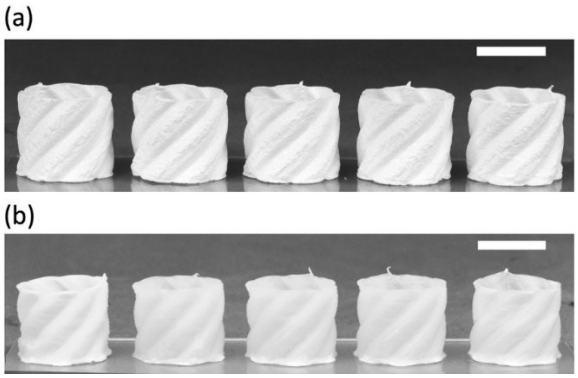

Supporting Fig. S7. Five 3D models printed consecutively by *ip*3DP. ABS45 was printed in (a) water and (b) ethanol. Scale bar = 1 cm.

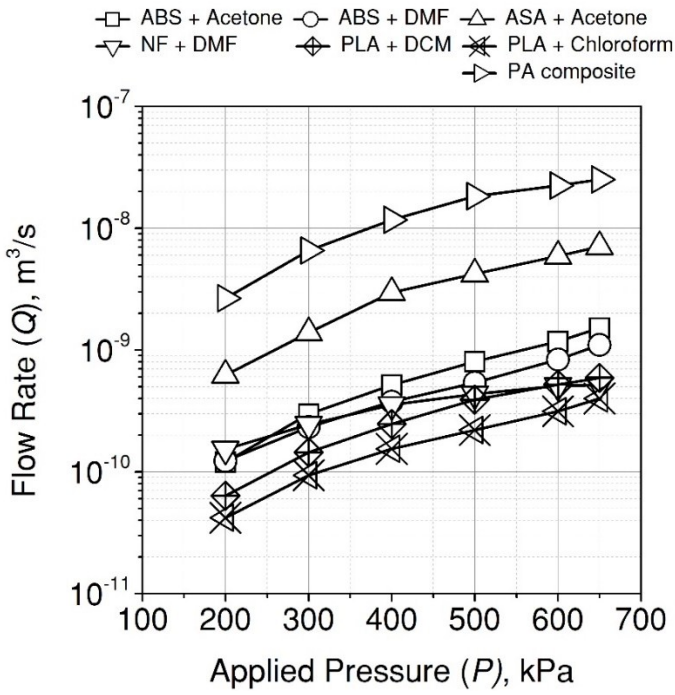

Supporting Fig. S8. A plot showing the process-related flow rate (Q) with respect to the applied pressure (P) for the polymer inks studied in this work.

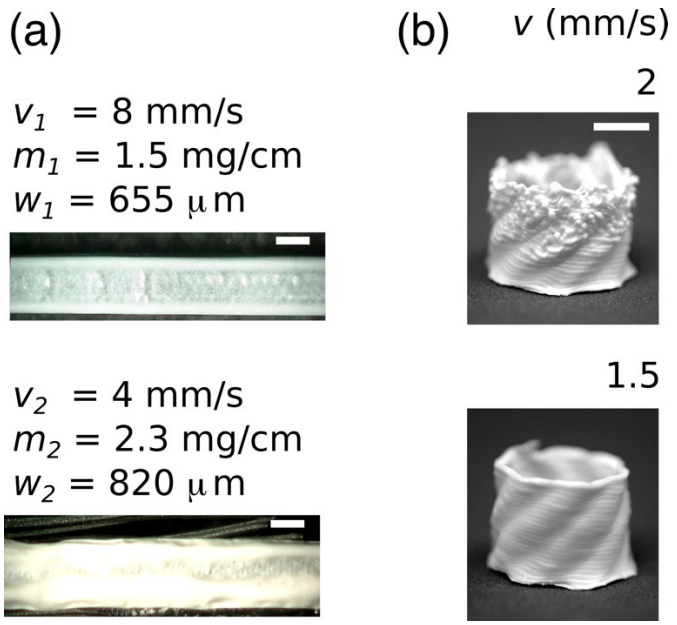

Supporting Fig. S9. Effects of print velocity (v) on the printed structures. (a) the width of the filament (w) and dispensed mass of the ink per unit length ($m=\dot{m}/v$). (b) Coil instability. The increase in v resulted in coil instability, affecting the print fidelity. Scale bar = 5 mm.

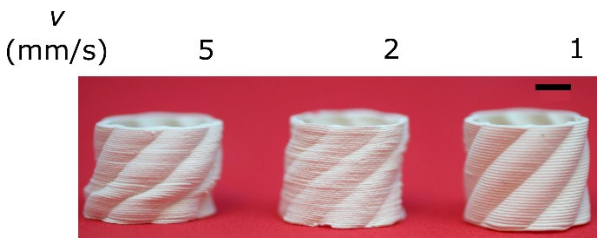

Supporting Fig. S10. Effect of print velocity (v) on the print fidelity of *ip*3DP with slow demixing of the solvent and the nonsolvent. At the high speed of the printing nozzle (v = 5 mm/s), the shear forced the printed structure tilted. Scale bar = 4 mm.

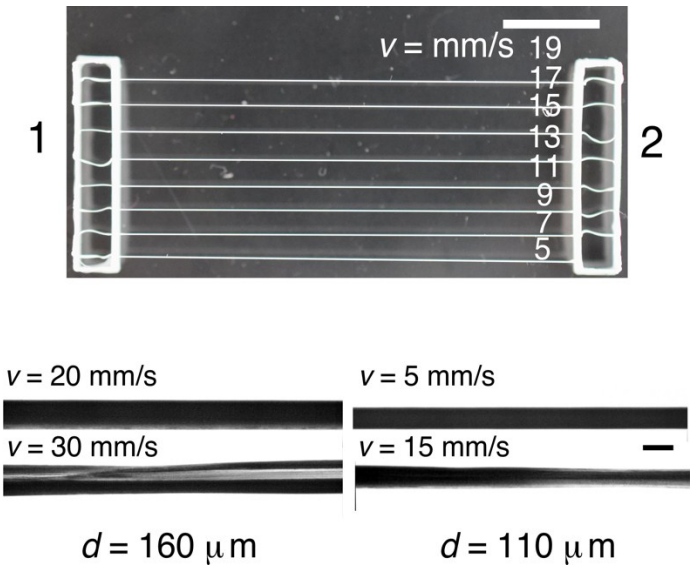

Supporting Fig. S11. An optical image showing the printed overhangs of ABS and microscopic images of the printed filaments with the variations of nozzle diameters and dispensing head velocities. Scale bars = (Top) 10 mm, (Bottom) 100 μm.

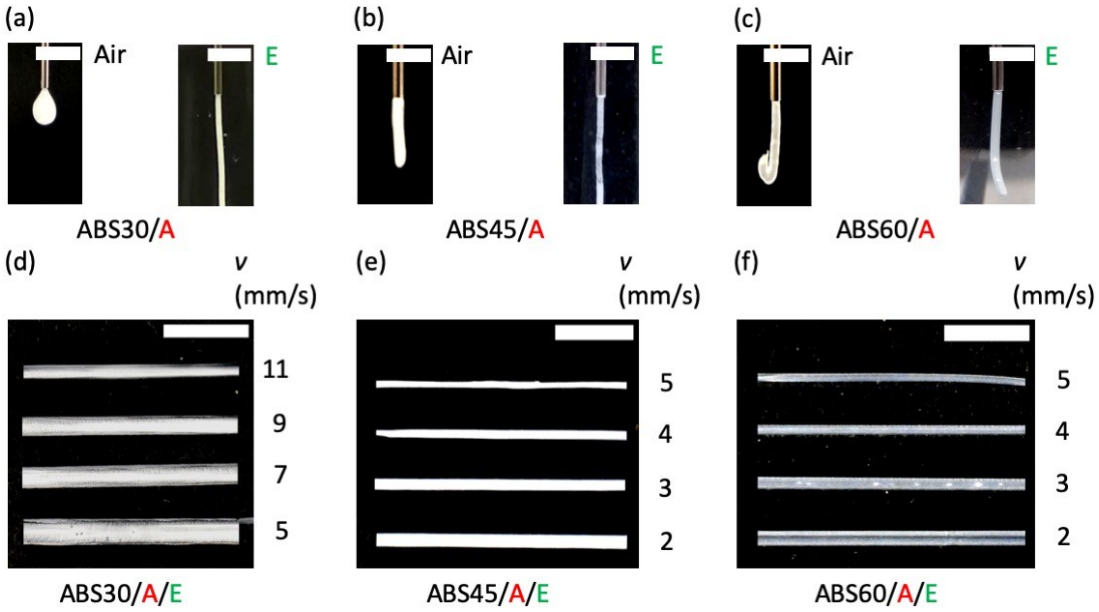

Supporting Fig. S12. Effect of surrounding media, air and ethanol, on the continuous filament formation when (a) ABS30, (b) ABS45, and (c) ABS60. The inks were dispensed through a nozzle. Fabrication of straight lines of (d) ABS30, (e) ABS45, and (f) ABS60 in ethanol at different dispensing head velocities (v). Scale bar = 5 mm.

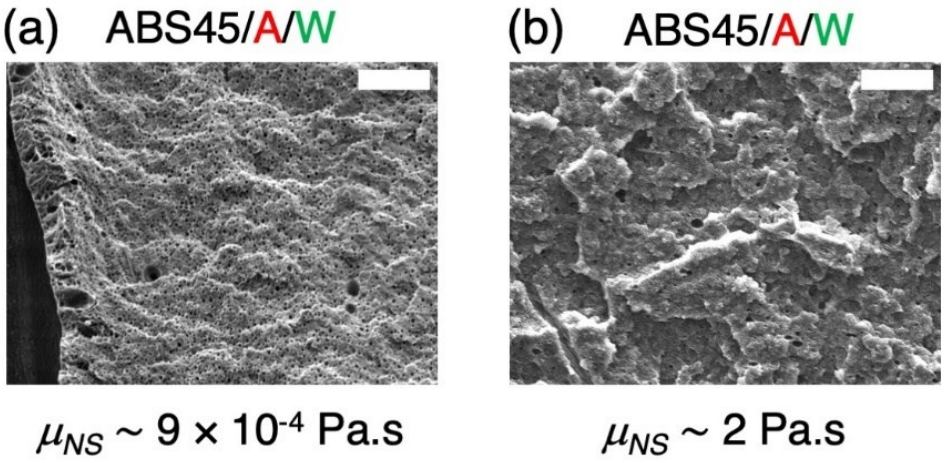

Supporting Fig. S13. (a) SEM image of the internal microstructure of the fracture surface of ABS45 printed in water (μ_{NS} ~ 9 × 10^{-4} Pa.s), exhibiting the micropores throughout the fracture surface. (b) SEM image of the internal microstructure of the fracture surface of ABS45 printed in water containing 1 % w/w of carboxymethyl cellulose (CMC) (μ_{NS} ~ 2 Pa.s), exhibiting rather dense surface. Scale bar = 20 μm.

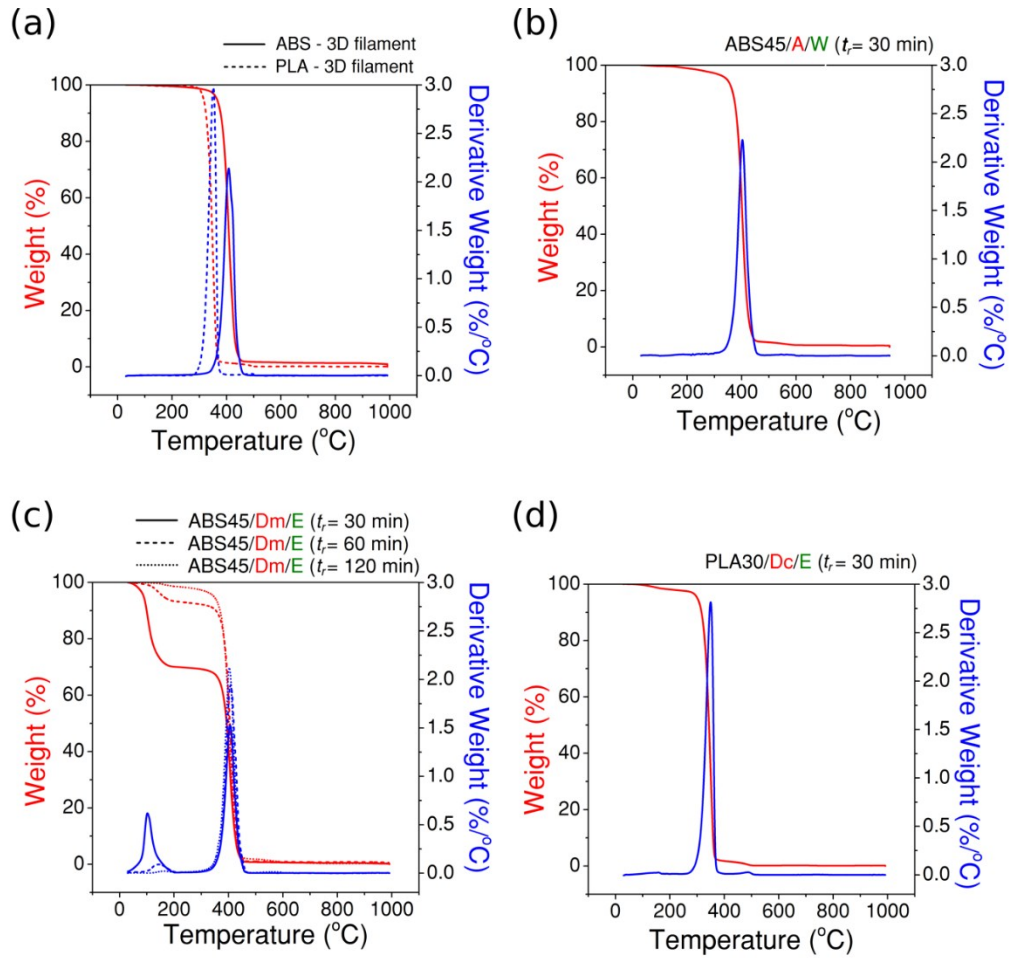

Supporting Fig. S14. Thermogravimetric analysis (TGA) to investigate presence of residual solvent or nonsolvent in the fabricated 3D structures by *ip*3DP. (a) Weight (%) and derivative of weight (%/°C) as a function of temperature of 3D filaments of ABS and PLA. (b) Weight (%) and derivative of weight (%/°C) as a function of temperature of ABS45 dissolved in acetone and printed in water with residence time of t_r = 30 min in water. (c) Weight (%) and derivative of weight (%/°C) as a function of temperature of ABS45 dissolved in DMF printed in ethanol with residence time of t_r = 30, 60 and 120 min in ethanol. (d) Weight (%) and derivative of weight (%/°C) as a function of temperature of PLA30 dissolved in DCM and printed in ethanol with residence time of t_r = 30 min in water.

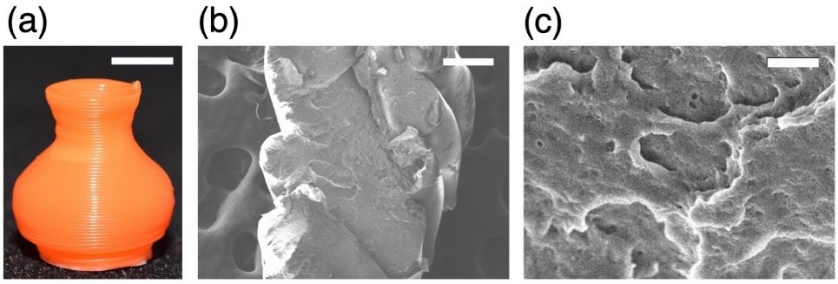

Supporting Fig. S15. PLA30 printed by *ip*3DP. (a) 3D structure, and (b-c) SEM images of microstructures of the fracture surface. Scale bars = a) 5 mm, b) 200 μm and c) 2 μm.

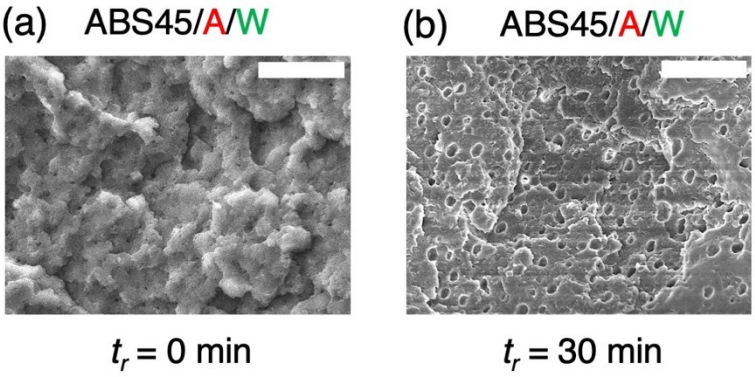

Supporting Fig. S16. Effect of residence time (t_r) on the micropores of the printed 3D models by *ip*3DP. (a) SEM image of the internal microstructure of the fracture surface of the ABS45 printed in water and immediately removed (t_r = 0 min) and dried in air. (b) SEM image of the internal microstructure of the fracture surface of the ABS45 printed in water and left for extraction of the solvents (t_r = 30 min). Scale bar = 10 μm.

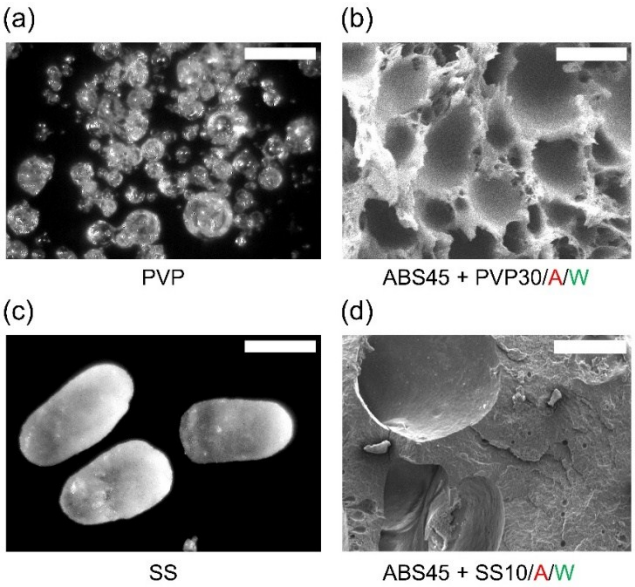

Supporting Fig. S17. Effect of porogens in the polymer ink on the microstructure. (a) Optical micrograph of polyvinylpyrrolidone (PVP) used as a porogen. (b) SEM image of the internal microstructure of the fracture surface of the ABS45 with PVP (30% of the weight of ABS) printed in water. (c) Optical micrograph of sodium sulphate (SS) used as a porogen. (d) SEM image of the internal microstructure of the fracture surface of the ABS45 with SS (10% of the weight of ABS) printed in water. Scale bars = (a) 300 μm, (b) 10 μm, (c) 300 μm, and (d) 100 μm.

Supporting Table S1. Polymers used in this study.

Sr. No.	Name	Abbreviation	Form	Supplier
1	High impact polystyrene	HIPS	Filament	SainSmart, USA
2	Polystyrene	PS	Food container	--
3	Acrylonitrile Butadiene Styrene	ABS	Filament/ Rod (5 mm dia.)	SainSmart, USA
4	Acrylonitrile Styrene Acrylate	ASA	Filament	SainSmart, USA
5	Polyethylene	PE	Petri dish	
6	Thermoplastic polyurethane	TPU	Filament	NinjaTek, USA
7	Polylactic Acid	PLA	Filament	Qidi Tech, China
8	Polycaprolactone	PCL	Pellet	Plastimake, Australia
9	Polyvinyl alcohol	PVA	Filament	SainSmart, USA
10	Polyacrylate composite	PA	Paste	Double-G, Singapore
11	Cellulose Acetate	CA	Powder	Sigma Aldrich, Singapore
12	Cellulose Acetate Propionate	CAP	Powder	Sigma Aldrich, Singapore
13	Cellulose Acetate Butyrate	CAB	Powder	Sigma Aldrich, Singapore

Supporting Table S2. Solvents and additives used in this study.

Sr. No.	Name	Abbreviation in the main text	Abbreviation in the figures	Form	Supplier
1	Acetone		A	Liquid	Sigma Aldrich, Singapore
2	Chloroform		Ch	Liquid	Sigma Aldrich, Singapore
3	Dichloromethane	DCM	Dc	Liquid	Fisher Scientific, Singapore
4	Dimethyl Formamide	DMF	Dm	Liquid	Fisher Scientific, Singapore
5	Dimethyl Sulfoxide	DMSO	Ds	Liquid	Fisher Scientific, Singapore
6	Ethanol		E	Liquid	Fisher Scientific, Singapore
7	Polyethylene Glycol (Mol. Wt. 300)	PEG	PEG	Liquid	Acros Organics, USA
8	Polyvinylpyrrolidone (Mol. Wt. 40000)	PVP	PVP	Powder	Sigma Aldrich, Singapore
9	Sodium Sulphate	SS	SS	Powder	Tokyo Chemical Industry Co. Ltd., Japan
10	Conductive Carbon Black	CC	CC	Powder	Ensaco, Imerys Graphite and Carbon, Belgium
11	Polyvinyl Alcohol Grade 1788L	PVA	PVA	Powder	Eastchem Lab, China
12	Laponite Clay EP Grade	LC	LC	Powder	BYK-Chemie GmbH, Germany
13	α-Cellulose	αC	αC	Powder	Sigma Aldrich, Singapore

Supporting Table S3. Formulations of inks (in w/w%) and corresponding nonsolvents for immersion precipitation used in this study.

Sr. No.	Polymer	Conc. (w/w%)	Solvent	Nonsolvent
1	HIPS	20-30	Acetone	Water, Ethanol
2	PS	25-30	Acetone, DMF	Water, Ethanol
3	ABS	20-60	Acetone, DMF, DCM	Water, Ethanol
4	ASA	45	Acetone	Ethanol
5	PE	20-30	Acetone, DCM	Water, Ethanol
6	TPU	20-30	DMF	Ethanol
7	PLA	20-30	DCM, Chloroform	Ethanol
8	PCL	50-60	DCM, Chloroform	Ethanol
9	PVA	30	Water	Acetone
10	PA	–	Water (as contained)	Acetone

Supporting Table S4. Elastic Modulus (E) and strength (σ) of the small dogbone coupons fabricated by *ip*3DP.

Polymer	Elastic modulus (E), GPa	Strength (σ), MPa
ABS60-*ip*3DP	1.45 ± 0.4	30 ± 1.8
ABS60-SC3DP	1.80 ± 0.2	35 ± 2.1
PLA30-*ip*3DP	1.32 ± 0.2	36 ± 1.5

Supporting Movie 1. *ip*3DP. Continuous patterning of an ink in a nonsolvent to form a 3D structure via immersion precipitation.

Supporting Movie 2. Diffusion of the solvent to the nonsolvent from the printed ink.

Polymer-solvent-nonsolvent ternary phase diagram. Ternary phase diagrams are useful in predicting suitability of a polymer solution of in a solvent to understand the phase inversion by immersion precipitation[1]. The corners in the phase diagram represent the pure components, and the three axes represent the binary combinations (Fig. S2). Any point inside the triangle indicates a ternary composition. The phase inversion causes separation of the ternary system into polymer-rich (high polymer concentration) (point *A* on binodal curve) and polymer-lean (low polymer concentration) (point *B* on binodal curve). The boundary which delimits this liquid-liquid demixing is termed as a bionodal curve (dashed curve). The binodal curve is the boundary between thermodynamically favorable set of conditions for a homogeneous polymer solution mixture (Region I) and the conditions favourable for phase separation (Region II, enclosed by the binodal curve). In the region II, the free energy of the mixture decreases by the phase separation. The bionodal curve can be obtained by the cloud points, representing the compositions at the bionodal curve, using rapid titration or turbidity measurement. When a polymer solution comes in contact with the nonsolvent, it follows a certain composition path in the ternary phase diagram. The liquid-liquid demixing can be instantaneous or delayed depending upon the short (crossing the bionodal curve fast) or long (crossing the binodal curve slow) composition path. This rate of liquid-liquid demixing determines the final morphology.

Effect of μ on *P*. For P = 300 kPa, the values of μ_{app} for ABS (45 % w/w in DMF) and PLA (30 % w/w in DCM) were 60 Pa.s and 180 Pa.s, respectively. When we obtained good print fidelity of the PLA ink at P_{PLA} = 600 kPa, the working pressure for the ABS ink is expected to be lower than P_{PLA} for the same printing conditions. The experiment was performed at P_{ABS} = 150 kPa. Overall, the values of μ_{app} allowed estimating the required pressure to achieve adequate mass flow rates to model 3D structures by *ip*3DP.

Extrusion of Inks through Nozzles. For a capillary of uniform d, the relationship between Q and P for a power law fluid is given by[2]:

$$Q = \frac{n\pi}{3n+1}\left(\frac{1}{2\mu}\frac{P}{l}\right)^{1/n} r^{3+1/n}$$

A simple analysis shows that for a Newtonian fluid (Poiseuille relationship), the fluidic resistance is inversely proportional to d^4. This relationship suggests that, when the nozzle diameter is reduced to the half, the new value of the pressure is 16 times as high as the original value to maintain the same rate of flow[2]. This restriction would pose practical challenges in handling high pressure. In this work, the applied pressure was limited to 650 kPa, and the use of the nozzles with large diameters (d = 410 – 680 μm) were preferred.

Effect of v on m and Δz. To characterize the effect of the speed of the dispensing head on the printed filaments, we first printed straight lines of 3-cm of ABS45 (45 w/w% of ABS in acetone) in water and measured the dispensed mass per unit length (m). For the given set of dispensing parameters, the increase in v resulted in the decrease in m and w (Fig. S7a); for the fixed mass flow rates, the faster motion of the syringe would result in the smaller amount ink deposited per unit length. Importantly, we found that the head speed v was an important parameter affecting the fidelity of printing. For *ip*3DP of ABS30 (30 w/w% in acetone) in ethanol, with printing parameters of (P, Δz, d) = (10 kPa, 0.4 mm, 410 μm), the filaments in two adjacent layers (in the vertical direction) did not attach properly for v = 2 mm/s. The unattached layers underwent rope-coil instability[3] and prevented adhesions between the deposited filaments (Fig. S7b). Proper attachment of the adjacent layers was observed for v = 1.5 mm/s (when all other parameters were maintained to be the same). The observation can be attributed to the difference in m and resulting difference in the cross-sectional dimensions of the printed filament; the extruded polymer ink must spread on the printed layer to ensure printability. In this example, the attachment between adjacent vertical layers were

compromised due to the smaller filament size resulting from the higher head speed. In such a case, adjustment of Δz would be required to ensure the stability of the 3D printed structures.

Effect of solvent-nonsolvent diffusion rate. Nonsolvents serve as another important variable to perform 3D modelling in *ip*3DP. In the setup of *ip*3DP, nonsolvents are the liquid media surrounding the printing head. We demonstrated that the print fidelity crucially depended on the solvent-nonsolvent diffusion rate. To highlight the effect of solvent-nonsolvent diffusion rate, we printed 3D structures of the PA composites (aqueous pastes) in acetone at three different dispensing head velocities (v) with printing parameters of (P, Δz, d) = (50 kPa, 0.2 mm, 620 μm) (Fig. S10). When the PA ink was printed at v = 5 mm/s and v = 2 mm/s, the obtained final 3D structure was not upright. The printed structure was upright only at v = 1 mm/s (Fig. S10). The diffusion coefficient (D_0) between acetone and water is 1.16×10^{-5} cm^2/s for acetone (solute) and water (solvent), and 4.56×10^{-5} cm^2/s for water (solute) and acetone (solvent)[4, 5]. We expect that the diffusion rate of water from the PA ink to acetone was lower than that of pure water to acetone. With slow diffusion between the solvent and nonsolvent, the printed structure would require time to complete solidification. In such cases, the motion of the dispensing head exerted shear forces and the resulting 3D structures were tilted. Generally, for the combination of solvents and nonsolvents with low diffusion rates (such as DCM and ethanol), v should be kept as low as possible to ensure sufficient time for the solidification of the printed filaments.

References

[1] L. Vogelaar, R. G. Lammertink, J. N. Barsema, W. Nijdam, L. A. Bolhuis-Versteeg, C. J. van Rijn, M. Wessling, *Small* **2005**, *1*, 645.

[2] F. Fang, S. Aabith, S. Homer-Vanniasinkam, M. K. Tiwari, in *3D printing in medicine*, (Ed: D. M. Kalaskar), Woodhead Publishing, **2017**, 167.

[3] G. Barnes, R. Woodcock, *Am. J. Phys.* **1958**, *26*, 205.

[4] D. R. Olander, *AIChE J.* **1961**, *7*, 175.

[5] D. R. Olander, *AIChE J.* **1963**, *9*, 207.